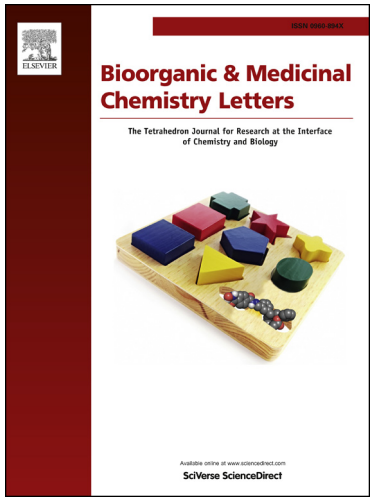

Discovery of 3,5-substituted 6-azaindazoles as potent pan-Pim inhibitors

Huiyong Hu, Xiaojing Wang, Grace Ka Yan Chan, Jae H. Chang, Steven Do, Jake Drummond, Allen Ebens, Wendy Lee, Justin Ly, Joseph P. Lyssikatos, Jeremy Murray, John G. Moffat, Qi Chao, Vickie Tsui, Heidi Wallweber, Aleksandr Kolesnikov

PII: S0960-894X(15)30086-X
DOI: http://dx.doi.org/10.1016/j.bmcl.2015.09.052
Reference: BMCL 23133

To appear in: *Bioorganic & Medicinal Chemistry Letters*

Received Date: 24 June 2015
Revised Date: 10 September 2015
Accepted Date: 22 September 2015

Please cite this article as: Hu, H., Wang, X., Chan, G.K.Y., Chang, J.H., Do, S., Drummond, J., Ebens, A., Lee, W., Ly, J., Lyssikatos, J.P., Murray, J., Moffat, J.G., Chao, Q., Tsui, V., Wallweber, H., Kolesnikov, A., Discovery of 3,5-substituted 6-azaindazoles as potent pan-Pim inhibitors, *Bioorganic & Medicinal Chemistry Letters* (2015), doi: http://dx.doi.org/10.1016/j.bmcl.2015.09.052

Bioorganic & Medicinal Chemistry Letters
journal homepage: www.elsevier.com

Discovery of 3,5-substituted 6-azaindazoles as potent pan-Pim inhibitors

Huiyong Hu [a], *Xiaojing Wang* [a], *Grace Ka Yan Chan* [a], *Jae H. Chang* [a], *Steven Do* [a], *Jake Drummond* [a], *Allen Ebens* [b], *Wendy Lee* [a], *Justin Ly* [a], *Joseph P. Lyssikatos* [c], *Jeremy Murray* [a], *John G. Moffat* [a], *Qi Chao* [d], *Vickie Tsui* [a], *Heidi Wallweber* [a], *Aleksandr Kolesnikov** [a]

[a] *Genentech, Inc., 1 DNA Way, South San Francisco, California 94080, United States.*
[b] *Juno Therapeutics, 307 Westlake Ave North, Seattle Washington 98109, United States*
[c] *Biogen Idec, 12 Cambridge Center, Cambridge, Massachusetts, 02142, United States*
[d] *BioMarin (Shanghai), Room 605 780 Cailun Road, Pudong District, Shanghai 201203*

ARTICLE INFO

Article history:
Received
Revised
Accepted
Available online

Keywords:
Pim kinases
Kinase inhibitor
Screening
Fragment based screen
Structure based drug design
Lead optimization

ABSTRACT

Pim kinase inhibitors are promising cancer therapeutics. Pim-2, among the three Pim isoforms, plays a critical role in multiple myeloma yet inhibition of Pim-2 is challenging due to its high affinity for ATP. A co-crystal structure of a screening hit **1** bound to Pim-1 kinase revealed the key binding interactions of its indazole core within the ATP binding site. Screening of analogous core fragments afforded 1*H*-pyrazolo[3,4-*c*]pyridine (6-azaindazole) as a core for the development of pan-Pim inhibitors. Fragment and structure based drug design led to identification of the series with picomolar biochemical potency against all three Pim isoforms. Desirable cellular potency was also achieved.

Pim (Proviral Insertion site for Moloney murine lymphomia virus) kinases are a family of three constitutively active, functionally related oncogenic serine/threonine protein kinases encoded by the genes *pim-1*, *pim-2*, and *pim-3*.[1] Pim overexpression has been observed in many cancers, and Pim kinases have drawn increased attention as promising targets for oncology drug therapeutics.[2] Reports on many pan Pim or Pim-1,3 selective inhibitors have been published recently.[3] Various studies have shown that, among the three Pim isoforms, Pim-2 expression is prevalent and highly critical to the growth and survival of multiple myeloma cancer cells,[4] yet inhibition of Pim-2 with an adenosine triphosphate (ATP) competitive Pim-2 inhibitor is challenging due to the high binding affinity of Pim-2 kinase to ATP.[5] We have previously reported the discovery of pyrazolo[1,5-*a*]pyrimidines as potent pan-Pim inhibitors achieving picomolar potencies against all three Pim kinases.[6] In this letter we report 1*H*-pyrazolo[3,4-*c*]pyridines as a distinct series with high pan-Pim inhibitory activities and moderate to high metabolic stability *in vivo*.

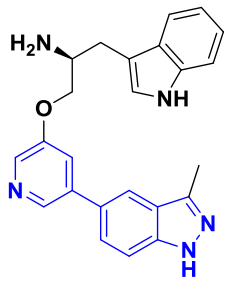

Pim-1 K_i = 14 nM, LE = 0.38, *Lip*E = 3.9
Pim-2 K_i = 8.7 nM, LE = 0.38, *Lip*E = 4.1
Pim-3 K_i = 17 nM, LE = 0.36, *Lip*E = 3.8

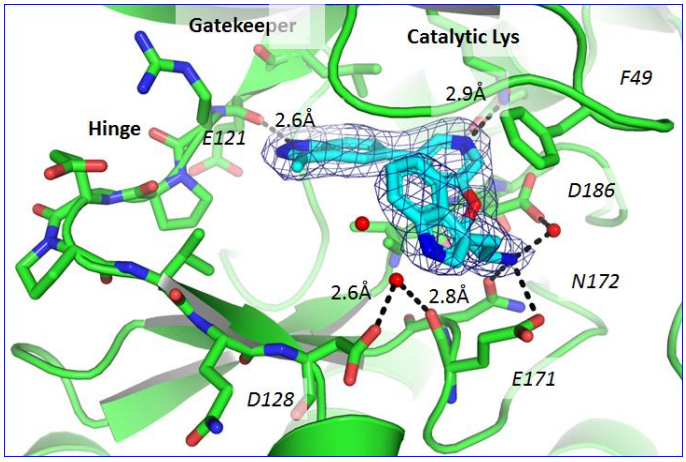

Figure1. X-ray co-crystal structure of **1** bound to Pim-1(PDB-ID 5DGZ).

The ATP binding site of PIM-1 is illustrated with compound **1** shown as cyan sticks, and the 2.5 Å resolution 2Fo-Fc electron density for compound **1** is represented as blue mesh contoured at 1sigma. Water molecules are represented as red spheres, hydrogen bond interactions between **1** and the protein are represented as black dashes. Important regions of the active site that are referred to in the text are labeled and the residues are shown as green sticks.

Screening of our internal compound collection identified indazole **1**, a known Akt inhibitor,[7] as a pan-Pim inhibitor with moderate potency. Having moderate LE[8] and *Lip*E (calculated with cLogP values),[9] compound **1** is equally potent for all three Pim isoforms. This was of particular interest because for the majority of scaffolds investigated, the inhibitory activity was often10-fold less for Pim-2 than for Pim-1 or Pim-3[6]. The X-ray co-crystal structure of **1** bound to full length Pim-1 (Figure 1) revealed several polar interactions in the ATP binding site including a single hydrogen bond interaction with the hinge residue Glu121, a contact of the pyridine nitrogen with the catalytic Lys67, and multiple interactions of the primary amine with Glu171, Asn172, and Asp186 (directly or through a conserved water). The benzene portion of the indole end group is exposed to the solvent front.

Table 1
Optimization of core motif based on compound **1**

ID		K_i [a] (μM) (*Lip*E [b])		
		Pim-1	**Pim-2**	**Pim-3**
2	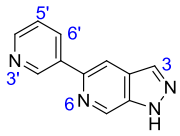	1.3 (4.2)	6 (3.5)	1.8 (4.0)
3	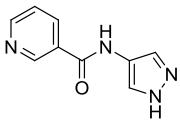	3.3 (5.3)	15 (4.6)	2.9 (5.3)
4	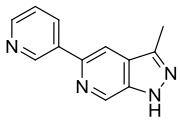	0.2 (4.9)	0.8 (4.3)	0.3 (4.7)
5	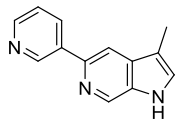	0.8 (3.8)	3.9 (3.1)	1.5 (3.5)
6	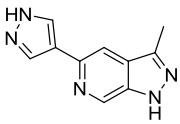	0.3 (5.2)	0.9 (4.7)	0.4 (5.1)
7	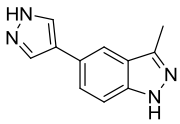	3.2 (3.3)	2.7 (3.4)	3.1 (3.3)
8	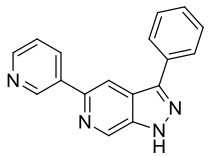	0.01 (4.7)	0.05 (4.0)	0.005 (5.0)
9	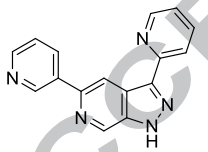	0.01 (5.5)	0.07 (4.7)	no data

[a] Biochemical assay. [b] *Lip*E = -log(Ki in molar) – cLogP.

Given the lead molecule **1** has a fairly extended structure we decided to pursue a fragment approach based on monitoring changes in *Lip*E. Starting from the indazole core of compound **1** (Fig. 1, in blue), we first made compound **2** (Table 1) with a nitrogen at the 6-position replacing the corresponding carbon in compound **1**. We hypothesized that incorporation of a nitrogen at the 6-position may establish a new hydrogen bond with a stable water observed in the vicinity.[6] Fragment **2** maintains decent *Lip*E comparable to compound **1** despite significant loss in potency. In order to reduce the number of aromatic rings for potential solubility gain, we also designed fragment **3** with an amide group replacing the fused pyridine moiety. Despite a 2-fold decrease in potency from compound **2** to **3**, lipophilic efficiency increases for the latter. Unfortunately, attempted potency gains based on fragment **3** proved to be elusive. Adding back a methyl group at C(3) of **2**, i.e. compound **4**, proved to be beneficial increasing

both potency by 6-fold and *Lip*E. To probe the importance of N(2) in azaindazole **4**, fragment **5** containing an azaindole core was made. The decreased potency is hard to explain considering the lack of hydrogen bond donor in the PIM-specific proline residue at the hinge to interact with N(2) of an azaindazole. However, similar structure activity relationship was seen with another scaffold we disclosed recently.[6] Replacing the pyridin-3'-yl head group at C(5) of **2** with a pyrazol-4'-yl moiety (compound **6**) proved to be a viable change resulting in similar potency and increased *Lip*E. Comparing with compound **7**, N(6) in compound **6** is accountable for 3- to 10-fold potency improvement and drastically increased *Lip*E. This observation validated our initial hypothesis of the benefit from an additional hydrogen bond to a conserved molecule of water. Following a potency boost by addition of a lipophilic methyl group at position 3 (e.g. compound **4**), further replacement with a phenyl or pyridin-2-yl group resulted in more than 100-fold potency improvement with concurrent *Lip*E increase (compounds **2 vs. 8** and **9)**. In summary, the novel 6-azaindazole core, as shown in **2**, **4**, **6**, **8** and **9** with improved *Lip*E in most cases provided a good starting point for further optimization.

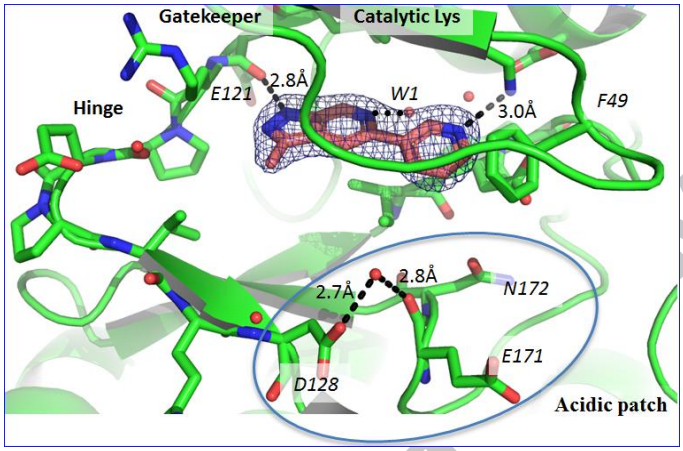

Figure2. X-ray crystal structure of PIM1 in complex with **4** (PDB-ID 5DHJ).
The ATP binding site of PIM1 is illustrated with compound **4** shown as salmon colored sticks, and the 2.46 Å resolution 2Fo-Fc electron density for **4** is represented as blue mesh contoured at 1sigma.

The X-ray co-crystal structure of compound **4** bound to Pim-1 and the key binding interactions of the fragment within the ATP binding pocket are illustrated in Figure 2. This includes hydrogen bonds between 1*H* and Glu121 at the hinge, N(6) and the adjacent conserved water W1 (3.1 Å) found in the kinase specificity pocket, finally N(3') and catalytic Lys67 of the backbone. Typical for Pim kinases are an abundant number of acidic residues (in this case are Asp128, Asn142, and Glu171) in the C-terminus; hence, this area is also referred to as the acidic patch. It is postulated that the acidic patch could be approached from two directions by basic moieties projecting from either the C(3) of the 1*H*-pyrazolo[3,4-*c*]pyridine core, or C(5') or C(6') of the 5-pyridinyl ring.

Table 2
Assembling 5-(Heteroaryl)-l*H*-pyrazolo[3,4-c]pyridine derivatives from three directions

ID		K_i [a] (μM) (*Lip*E [b])			ID		K_i (μM) (*Lip*E)		
		Pim-1	**Pim-2**	**Pim-3**			**Pim-1**	**Pim-2**	**Pim-3**
4	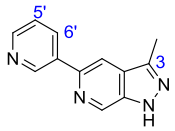	0.2 (4.9)	0.8 (4.3)	0.3 (4.7)	**13**	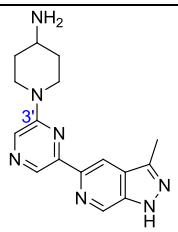	0.006 (6.7)	0.17 (5.3)	0.009 (6.6)
10	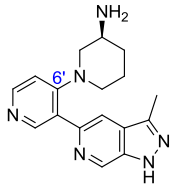	3.5 (3.5)	8.3 (3.1)	5 (3.3)	**14**	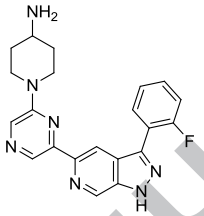	0.0001 (6.8)	0.003 (5.3)	0.0001 (6.9)
11	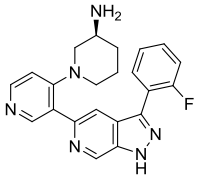	0.014 (4.2)	0.035 (3.9)	0.006 (4.6)	**15**	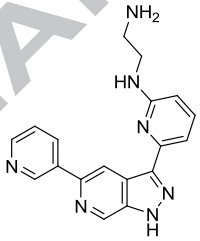	0.0003 (7.6)	0.003 (6.6)	0.0002 (7.9)
12	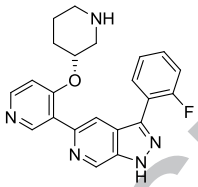	0.0034 (6.0)	0.0017 (5.3)	0.00011 (6.5)	**16**	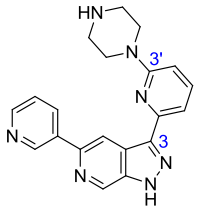	0.00004 (8.1)	0.0005 (7.0)	0.00001 (8.7)

[a, b] As in Table 1.

Even though compound **10** can be modeled such that the basic amine reaches the acidic patch (data not shown), this compound incurred significant potency and *Lip*E loss. This is likely because the piperidine ring would need to be co-planar with the pyridine in order for the salt bridge to acidic residues to form, whereas an orthogonal conformation that does not fit in the narrow pocket would be preferred in solution. The next step was an addition of a hydrophobic 2'-fluorophenyl group at C(3) in compound **11** which caused a significant potency gain with improvement in *Lip*E. Insertion of an oxygen spacer at C(6'), i.e. compound **12**, gave rise to further potency gains, this time likely due to a preference to adopt co-planar geometry in solution. Compounds **13** and **14** approach the acidic patch from a different position (C(3') of the 5-pyrazine-2'-yl ring). Such analogs retained planarity of the scaffold, and good potency was achieved with picomolar K_i's for Pim-1 and Pim-3, and single-digit nanomolar K_i for Pim-2, as exemplified by **14**.[11] Compounds **15** and **16** interact with the acidic patch from the opposite side of

the core. Compound **15** with a flexible amino group bearing chain is equipotent to compound **14** yet shows improved *Lip*E for all Pim isoforms, indicating the promise of utilizing the 2-pyridine as a spacer group. Restraining the flexibility of a basic amine in compound **16** resulted in further improvement in potency. For the first time, subnanomolar K_i was achieved for Pim-2 in the 6-azaindazole series, prompting us to focus our efforts on expanding SAR for the series.

Table 3
Probing catalytic Lysine interactions

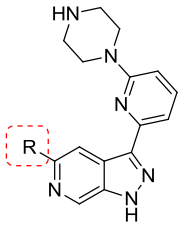

ID	R	K_i [a] (nM) (*Lip*E[b])			ID	R	K_i (nM) (*Lip*E)		
		Pim-1	Pim-2	Pim-3			Pim-1	Pim-2	Pim-3
17		0.041 (7.6)	0.30 (6.7)	0.037 (7.6)	**24**		171 (6.8)	1100 (6.0)	115 (7.0)
18		0.010 (9.2)	0.049 (8.5)	0.010 (9.2)	**25**		2.0 (7.7)	1.1 (8.0)	0.68 (8.2)
19	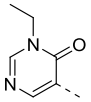	0.015 (10.5)	0.145 (9.5)	0.070 (10.9)	**26**	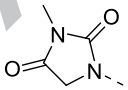	31 (6.4)	33 (6.4)	3.3 (7.4)
20		0.036 (8.5)	0.58 (7.3)	0.017 (8.9)	**27**		8.5 (6.6)	82 (5.6)	no data (no data)
21	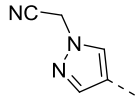	0.022 (9.2)	0.127 (8.4)	0.013 (9.4)	**28**		4.0 (6.5)	26 (5.7)	1.0 (7.1)
22	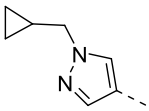	0.021 (8.0)	0.253 (6.9)	0.016 (8.1)	**29**	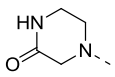	13 (7.3)	17 (7.2)	1.4 (8.3)
23		1.82 (7.1)	5.4 (6.7)	0.65 (7.6)	**30**		3.3 (6.9)	14 (6.3)	4.4 (6.8)

[a] As in Table 1.

A variety of head groups aimed to form polar interactions with Lys67 have been tested (Table 3). Substituents at C(5') of the 5-pyridine-3'-yl ring are tolerated as shown in compound **17,** which is equipotent to its unsubstituted counterpart **16**. The presence of a second nitrogen, i.e. N(2') in 6'-methylpyrazine-2-yl (compound **18),** was hypothesized to restrict the rotation of pyrazine-azaindazole bond and maintain a more preferable biologically active conformation. Indeed, excellent picomolar potency was achieved for all three Pim kinases. The same consideration can be applied to compound **19** containing hydrophilic pyrimidinone group and showing highest *Lip*E in the series. A variety of substituents attached to the second nitrogen of the pyrazole head group (compounds **20**- **22**) are tolerated, providing a handle for adjusting physicochemical properties of the compounds.

Attempt to replace pyrazole with imidazole led to a significant loss of potency in compound **23** presumably due to a combination of losing the methyl group, which has van der Waals interaction with Phe49, and different charge distributions caused by the heterocycles (Figure 1S in Supplemental Materials) whose exact contributions to potency are unknown. Compound **24** bearing aliphatic amide as a head group has much reduced potency (K_i in the micromolar range for Pim-2). When the alkyl amide group is replaced by the corresponding urea in compound **25**, the potency was restored to the low nanomolar range possibly due to an internal hydrogen bond formation placing the carbonyl closer toward the catalytic lysine. Our further attempts to utilize oxygen as the hydrogen bond acceptor were not successful. Compounds with a head group such as imidazolidindione (compound **26**), tetrahydrofuran or tetrahydropyran (compounds **27** and **28**, respectively), piperazinone (compound **29**), and morpholine (compound **30**) are all not well tolerated. In general, heteroaromatic head groups proved to be beneficial for potency, and therefore N-methylpyrazolyl group at C(5) was selected to explore structure-activity relationship by varying amino-bearing groups connected to C(3) of the core and interacting with the acidic patch (Table 4)

Table 4
Exploring basic groups to access the acidic patch.

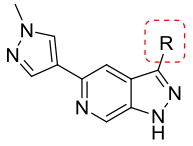

ID	R	K_i [a] (nM) (*Lip*E[b])			ID	R	K_i (nM) (*Lip*E)		
		Pim-1	Pim-2	Pim-3			Pim-1	Pim-2	Pim-3
31	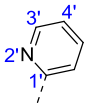	7.7 (6.2)	48 (5.4)	3.7 (6.5)	**35**	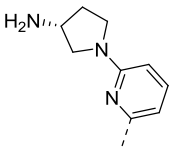	0.14 (7.8)	0.72 (7.0)	0.021 (8.6)
20	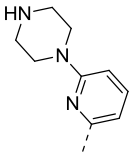	0.036 (8.5)	0.58 (7.3)	0.017 (8.9)	**36**	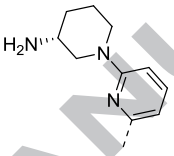	0.035 (8.0)	0.43 (6.9)	0.015 (8.3)
32	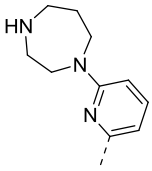	0.020 (7.9)	0.17 (7.0)	0.013 (8.1)	**37**	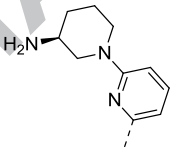	0.060 (7.7)	0.26 (7.1)	0.015 (8.3)
33	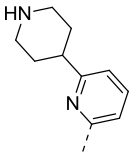	0.22 (7.4)	2.2 (6.5)	0.12 (7.7)	**38**	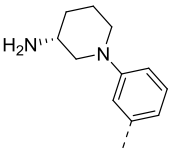	0.39 (6.3)	1.25 (4.8)	0.29 (6.4)
34	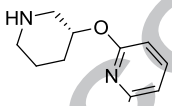	0.27 (6.8)	6.2 (5.4)	0.16 (7.0)	**39**	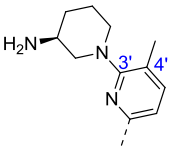	0.013 (7.9)	0.088 (7.1)	0.006 (8.2)

[a] As in Table 1.

Different substitutions at C(3') off the pyridine ring via linkers such as nitrogen, carbon or oxygen were studied. Compound **20** with piperazine moiety at C(3') is 80 to 200-fold more potent than compound **31** without any substitution. Homopiperazine derivative **32** is slightly more potent, yet has lower *Lip*E value indicating improved potency is driven mostly likely by increased lipophilicity. The carbon linked compound **33**, however, is 4- to 7-fold less active than compound **20**. It is likely due to a conformational change caused by the sp^3-hybridized carbon attached to C(3'), resulting in a shift of the basic amine away from the acidic patch. Similarly, compound **34** with an oxygen linker may have lost potency relative to the nitrogen linker due to

differences in preferred conformations driven by dipole-dipole interaction between oxygen linker and pyridine nitrogen. In order to optimize the interaction with the acidic patch, primary amines were also investigated. For example, compounds **35** and **36** contain primary amines linked by a five- and six-membered heterocyclic ring, respectively. Both ring sizes are tolerated, while the six-membered ring is more favorable for potency. Equal potency of enantiomers **36** and **37** shows the ability of the acidic patch to accommodate both. The importance of the nature of the spacer between the core and a basic amine bearing group is clearly demonstrated by the difference in potency between compounds **36** and **38**. While compound **36** contains a pyridinyl moiety constrained by intramolecular interactions to prefer the bound conformation, free rotation of the benzene ring in compound **38** gives likely no statistical preference for a bioactive conformation and resulted in a drop of potency. The installation of methyl group at the C(4') position of the pyridine ring in compound **39** was aimed to further enforce an orthogonal orientation of the piperidine ring, consequently positioning a primary amine in the vicinity of the acidic patch. As a result, 2- to 4-fold potency improvement was observed from compound **37** to **39,** accompanied by small increase in *Lip*E value for Pim-1. In general, it is worth noting that high *Lip*E values (> 7 for Pim-2 and > 7.5 for Pim-1 and Pim-3) were consistently observed within the basic amine containing subseries, such as compounds **16**, **20, 32, 35-37 and 39.**

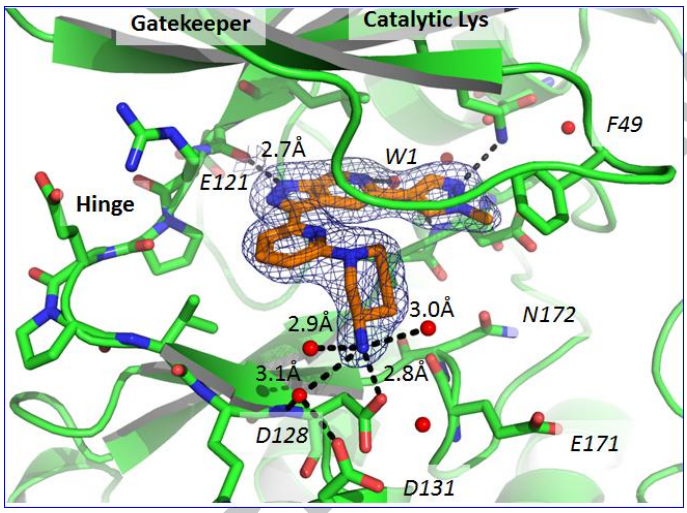

Figure 3. X-ray crystal structure of PIM1 in complex with compound **36** (PDB-ID 5DIA).
The ATP binding site of PIM1 is illustrated with compound **36 s**hown as orange colored sticks, and the 1.9 Å resolution 2Fo-Fc electron density for **36** is represented as blue mesh contoured at 1sigma.

Shown in Figure 3 is the X-ray co-crystal structure of compound **36** bound to Pim-1. As expected, a hydrogen bond was seen between the carbonyl oxygen of hinge residue Glu121 and 1*H* of the 6-azaindazole core. N(6) of the core acted as an acceptor to form a hydrogen bond with adjacent molecule of water (3.0 Å). A third hydrogen bond was observed between N(4') of the pyrazole and Lys67. The basic amine formed one direct salt bridge to the acidic residue and additional hydrogen bonds with water molecules simultaneously.

Table 5
Profile of compound **40**

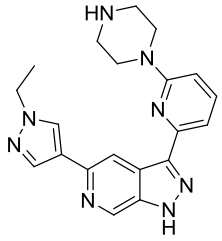

40
Pim-1 K_i = 0.073 nM
Pim-2 K_i = 0.473 nM
Pim-3 K_i = 0.041 nM

Cellular Potency IC_{50} (μM)				ADME Properties (Rat)					
BaF3_IL3	**BaF3_Pim**	**Ratio** [a]	**MM1.s**	**CLp** [b]	**%F** [c]	**%PPB** [d]	**RLM CLint** [e]	**$MDCK_{A-B}$** [f]	**MDCK $_{ratio}$** [g]
5.4	0.077	70	0.64	14	1	97.8	150	0.5	51

[a] Ratio = BaF3_IL3 IC_{50}/BaF3_Pim-1 IC_{50}. [b] CLp=*in vivo* plasma clearance (mL/min/kg). [c] Oral bioavailability. [d] Plasma Protein Binding. [e] CLint=intrinsic clearance from rat liver microsomes (mL/min/kg). [f] Apparent permeability (x10^{-6}cm/sec). [g] MDCK ratio = B-A/A-B.

After triaging compounds through the testing cascade, compound **40** (Table 5) provided the most balanced profile in terms of potency and stability *in vivo* as one of the lead compounds of the series. It shows double-digit nanomolar potency when tested for cell-killing activity against PIM1-transfected BaF3 myeloid cells, whose survival in the absence of added IL-3 is Pim-1 dependent. However, it is not potent against the parental BaF3 cell line, whose growth and survival is dependent on IL-3 but independent of Pim kinase functions. The cellular potency (IC_{50}) ratio between these cell lines is about 70-fold, demonstrating the absence of non-selective cytotoxicity. Compound **40** has also potent antiproliferative activity against the MM1.S multiple myeloma cell line, with IC_{50} of 0.64 μM. Despite low total clearance the poor bioavailability of compound **40** has likely resulted from poor permeability (indicated by the MDCK measurements) and possibly high intestinal metabolism. This liability prompted us to design another series of analogs solving this type of metabolism issues, which will be reported in due time.

Scheme 1. Synthesis of **40**

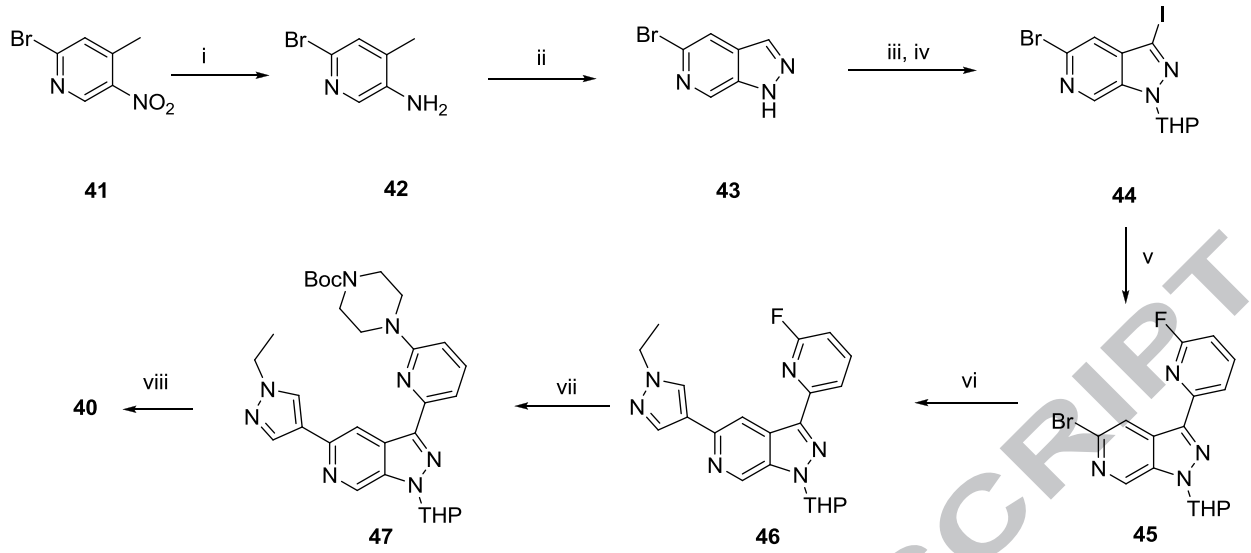

[a] Reagents and conditions: (i) Zn, NH_4Cl, EtOH, water, rt (60%); (ii) $NaNO_2$, AcOH, 0 °C to rt (73%); (iii) N-iodosuccinimide, DMF, 0 °C to rt (85%); (iv) DHP, *p*-TSA, CH_2Cl_2, 24h (67%); (v) 2-fluoro-6-(tributylstannyl)pyridine, $Pd(PPh_3)_4$, toluene, 110 °C, 3h (84%); (vi) 1-ethyl-4-(4,4,5,5-tetramethyl-1,3,2-dioxaborolan-2-yl)-1H-pyrazole, $Pd(PPh_3)_2Cl_2$, Na_2CO_3, 1,4-dioxane, reflux (80%); (vii) Boc-piperazine, DMSO, 105 °C, 48h, (95%); (vii) 4M HCl in 1,4-dioxane, MeOH, rt (85%).

The synthesis of 6-azaindazole analogs is exemplified in Scheme 1.[12] Zinc reduction of the nitro group of compound **41** afforded amine 42**.** Treating **42** with sodium nitrite in acetic acid led to the formation of 6-azaindazole **43**, which was iodinated and then protected by THP group to afford **44**. Stille coupling between **44** and 2-fluoro-6-(tributylstannyl)pyridine provided key intermediate **45**. Suzuki coupling between bromide **45** and aryl boronic acid or boronate (exemplified by 1-ethyl-4-(4,4,5,5-tetramethyl-1,3,2-dioxaborolan-2-yl)-1H-pyrazole in Scheme 1) afforded **46.** Subsequent SnAr displacement with various monoprotected diamines (exemplified by Boc-piperazine in Scheme 1) followed by acidic deprotection yielded final compounds represented by **40** in Scheme **1**.

In summary, based on the X-ray co-crystal structure of the screening hit **1** with Pim-1, an indazole core was identified as the starting point. A fragment based approach to screen similar fragments afforded 6-azaindazoles as one of the desirable cores. Further optimizations yielded analogs with picomolar biochemical potency against all three Pim kinases, resulting in good cellular potency. Poor pharmacokinetic properties for the 6-azaindazole series prompted us to design alternative Pim inhibitors that successfully solved the problems. We will report the improved series in due time.

Acknowledgments

We are grateful to analytical, purification chemistry and compound management group for compound characterization, purification and handling. Thanks to Vivienne Allen for the conformational analysis.

References and notes

1. (a) Cuypers, H. T.; Selten, G.; Quint, W.; Zijlstra, M.; Maandag, E. R.; Boelens, W.; van Wezenbeek, P.; Melief, C.; Berns, A. *Cell* **1984**, *37*, 141; (b) Selten, G.; Cuypers, H. T.; Berns, A. *EMBO J.* **1985**, *4*, 1793; (c) van Lohuizen, M.; Verbeek, S.; Scheijen, B.; Wientjens, E.; van der Gulden, H.; Berns, A. *Cell* **1991**, *65*, 737.

2. (a) Magnuson, N. S.; Wang, Z.; Ding, G.; Reeves, R. *Future Oncol.* **2010**, *6*, 1461-1478; (b) Merkel, A. L.; Meggers, E.; Ocker, M. *Expert Opin. Investig. Drugs* **2012**, *21*, 425.
3. (a) Tao, Z.-F.; Hasvold, L. A.; Leverson, J. D.; Han, E. K.; Guan, R.; Johnson, E. F.; Stoll, V. S.; Stewart, K. D.; Stamper, G.; Soni, N.; Bouska, J. J.; Luo, Y.; Sowin, T. J.; Lin, N.-H.; Giranda, V. S.; Rosenberg, S. H.; Penning, T. D. *J. Med. Chem.* **2009**, *52*, 6621; (b) Pastor, J.; Oyarzabal, J.; Saluste, G.; Alvarez, R. M.; Rivero, V.; Ramos, F.; Cendon, E.; Blanco-Aparicio, C.; Ajenjo, N.; Cebria, A.; Albarran, M. I.; Cebrian, D.; Corrionero, A.; Fominaya, J.; Montoya, G.; Mazzorana, M. *Bioorg. Med. Chem. Lett.* **2012**, *22*, 1591; (c) Tsuhako, A. L.; Brown, D. S.; Koltun, E. S.; Aay, N.; Arcalas, A.; Chan, V.; Du, H.; Engst, S.; Franzini, M.; Galan, A.; Huang, P.; Johnston, S.; Kane, B.; Kim, M. H.; Laird, A. D.; Lin, R.; Mock, L.; Ngan, I.; Pack, M.; Stott, G.; Stout, T. J.; Yu, P.; Zaharia, C.; Zhang, W.; Zhou, P.; Nuss, J. M.; Kearney, P. C.; Xu, W. *Bioorg. Med. Chem. Lett.* **2012**, *22*, 3732; (d) Xiang, Y.; Hirth, B.; Asmussen, G.; Biemann, H.-P.; Bishop, K. A.; Good, A.; Fitzgerald, M.; Gladysheva, T.; Jain, A.; Jancsics, K.; Liu, J.; Metz, M.; Papoulis, A.; Skerlj, R.; Stepp, J. D.; Wei, R. R. *Bioorg. Med. Chem. Lett.* **2011**, *21*, 3050; (e) Dakin, L. A.; Block, M. H.; Chen, H.; Code, E.; Dowling, J. E.; Feng, X.; Ferguson, A. D.; Green, I.; Hird, A. W.; Howard, T.; Keeton, E. K.; Lamb, M. L.; Lyne, P. D.; Pollard, H.; Read, J.; Wu, A. J.; Zhang, T.; Zheng, X. *Bioorg. Med. Chem. Lett.* **2012**, *22*, 4599; (f) Burger, M. T.; Han W.; Lan, J.; Naguchi, G.; Bellamacina, C.; Lindval, M.; Atallah, G.; Ding, Y.; Mathur, M.; McBride, C.; Beans, E. L.; Muller, K.; Tamez, V.; Zhang, Y.; Huh, K.; Feucht, P.; Zavorotinskaya, T.; Dai, Y.; Holash, J.; Castillo, J.; Langowski J., Wang Y.; Chen M. Y.; Garcia P. *ACS Med. Chem.* **2013**, *4*, 1193; (g) Casuscelli, F.; Ardini, E.; Avanzi, N.; Casale, E.; Cervi, G.; D'Anello, M.; Donati, D.; Faiardi, D.; Ferguson, R. D.; Fogliatto, G.; Galvani, A.; Marsiglio, A.; Mirizzi, D. G.; Montemartini, M.; Orrenius, C.; Papeo, G.; Piutti, C.; Salom, B.; Felder, E. R. *Bioorg. Med. Chem. Lett.* **2013**, *21*, 7364; (h) Dwyer, Michael M. P.; Keertikar, K.; Paruch, K.; Alvarez, C.; Labroli, M.; Poker, C.; Fischmann, T. O.; Mayer-Ezell, R.; Bond, R.; Wang, Y.; Azevedo, R.; Guzi, T. J. *Bioorg. Med. Chem. Lett.* **2013**, *23*, 6178; (i) Wurz, R. P.; Pettus, L. H.; Jackson, C.; Wu, B.; Wang, H.; Herberich, B.; Cee, V.; Lanman, B. A.; Reed, A. B.; Chavez, F., Jr.; Nixey, T.; Laszlo, J., III; Wang, P.; Nguyen, Y.; Sastri, C.; Guerrero, N.; Winston, J.; Lipford, J. R.; Lee, M. R.; Andrews, K. L.; Mohr, C.; Xu, Y.; Zhou, Y.; Reid, D. L.; Tasker, A. S. *Bioorg. Med. Chem. Lett.* **2015**, *25*, 847; (j) Ishchenko, A.; Zhang, L.; Le Brazidec, J.; Fan, J.; Chong, J. H.; Hingway, A.; Raditsis, A.; Singh, L.; Elenbaas, B.; Hong, V. S.; Marcotte, D.; Silvian, L.; Enyedy, I.; Chao, J. *Bioorg. Med. Chem. Lett.* **2015**, *25*, 474; (k) Wang, H.; Cee, V. J.; Chavez, F.; Lanman, B. A.; Reed, A. B.; Wu, B.; Guerrero, N.; Lipford, J. R.; Sastri, C.; Winston, J.; Andrews, K. L.; Huang, Xin; L., Matthew R.; Mohr, C.; Xu, Y.; Zhou, Y.; Tasker, A. S. *Bioorg. Med. Chem. Lett.* **2015**, *25*, 834; (l) Wu, B.; Wang, H.; Cee, V. J.; Lanman, B. A.; Nixey, T.; Pettus, L.; Reed, A. B.; Wurz, R. P.; Guerrero, N.; Sastri, C.; Winston, J.; Lipford, J. R.; Lee, M. R.; Mohr, C.; Andrews, K. L.; Tasker, A. S. *Bioorg. Med. Chem. Lett.* **2015**, *25*, 775.
4. (a) Munugalavadla, V.; Berry, L.; Chen, Y.-H.; Deshmukh, G.; Drummond, J.; Du, C.; Eby, M.; Fitzgerald, K.; Friedman, L. S.; Gould, S. E.; Kenny, J. R.; Maecker, H.; Moffat, J.; Moskalenko, M.; Pacheco, P.; Saadat, A.; Slaga, D.; Sun, L.; Wang, X.; Yang, Y.; Ebens, A. J. *Blood* **2010**, *116*, 4084; (b) Ebens, A. J.; Berry, L.; Chen, Y.-H.; Deshmukh, G.; Drummond, J.; Du, C.; Eby, M.; Fitzgerald, K.; Friedman, L. S.; Gould, S. E.; Kenny, J. R.; Maecker, H.; Moffat, J.; Moskalenko, M.; Pacheco, P.; Saadat, A.; Slaga, D.; Sun, L.; Wang, X.; Yang, Y.; Munugalavadla, V. *Blood* **2010**, *116*, 3001; (c) Drygin, D.; Haddach, M.; Pierre, F.; Ryckman, D. M. *J. Med. Chem.* **2012**, *55*, 8199; (d) Anizon, F. S., Shtil, A. A.; Danilenko, V.N.; Moreau, P. *Curr. Med. Chem.* **2010**, *17*, 4114; (e) Morwick, T. *Expert Opin. Ther. Pat.* **2010**, *20*, 193.
5. Garcia, P. D.; Langowski,J. L.; Wang, Y; Chen M., Castillo J.; Fanton, C.; Ison, M; Zavorotinskaya,T.; Dai, Y.; Lu, J.; Niu, X-H.; Basham, S.; Chan, J; Yu, J.; Doyle, M.; Feucht, P.; Warne, R.; Narberes, J.; Tsang, T.; Fritsch, C.; Kauffmann, A.; Pfister, E.; Drueckes, P.; Trappe, J.; Wilson, C.; Han, W.; Lan, J.; Nishiguchi,G.; Lindvall, M.; Bellamacina, C.; Alex Aycinena, J.; Zang, R.; Holash, J.; Matthew T. Burger, M. T. *Clin. Cancer Res.* **2014**, *20*, 1834.
6. Wang, X.; Magnuson, S.; Pastor, R.; Fan, E.; Hu, H.; Tsui, V.; Deng, W.; Murray, J.; Steffek, M.; Wallweber, H.; Moffat, J.; Drummond, J.; Chan, G.; Harstad, E.; Ebens, A. J. *Bioorg. Med. Chem. Lett.* **2013**, *23*, 3149.
7. (a) Woods, K. W.; Fischer, J. P.; Claiborne, A.; Li, T.; Thomas, S. A.; Zhu, G. -D.; Diebold, R. B.; Liu, X.; Shi, Y.; Klinghofer, V.; Han, E. K.; Guan, R.; Magnone, S. R.; Johnson, E. F.; Bouska, J. J.; Olson, A. M.; de Jong, R.; Oltersdorf, T.; Luo, Y.; Rosenberg, S. H.; Giranda, V. L.; Li, Q. *Bioorg. Med. Chem.* **2006**, *14*, 6832; (b) Luo, Y.; Shoemaker, A. R.; Liu, X.; Woods, K. W.; Thomas, S. A.; de Jong, R.; Han, E. K.; Li, T.; Stoll, V. S.; Powlas, J. A.; Oleksijew, A.; Mitten, M. J.; Shi, Y.; Guan, R.; McGonigal, T. P.; Klinghofer, V.; Johnson, E. F.; Leverson, J. D.; Bouska, J. J.; Mamo, M.; Smith, R. A.; Gramling-Evans, E. E.; Zinker, B. A.; Mika, A. K.; Nguyen, P. T.; Oltersdorf, T.; Rosenberg, S. H.; Li, Q.; Giranda, V. L. *Mol. Cancer Ther*. **2005**, *4*, 977.
8. LE: Ligand efficiency = -1.4*log(Ki in molar)/(no. of heavy atoms). Hopkins, A. L.; Groom, C. R.; Alex, A. *Drug Discovery Today* **2004**, *9*, 430.
9. (a) Leeson P. D.; Springthorpe, B. *Nature Rev. Drug Discovery.* **2007**, *6*, 881; (b) Shultz, M. D. *Bioorg. Med. Chem. Lett.* **2013**, *23*, 5980.
10. Gerber, P. R.; Mfiller, K. *J. Comput. Aided Mol. Des.* **1995**, *9*, 251.
11. Synthesis of selected compounds **11**, **12**, and **14** is shown in Scheme 1S in supplemental material.
12. Synthesis of **39** is shown in Scheme 2S in supplemental material.

Graphical Abstract

.

Discovery of 3,5-substituted 6-azaindazoles as potent pan-Pim inhibitors

Leave this area blank for abstract info.

Huiyong Hu, Xiaojing Wang, Grace Ka Yan Chan, Jae H. Chang, Steven Do, Jake Drummond, Allen Ebens, Wendy Lee, Justin Ly, Joseph Lyssikatos, Jeremy Murray, John G. Moffat, Qi Chao, Vickie Tsui, Heidi Wallweber, Aleksandr Kolesnikov

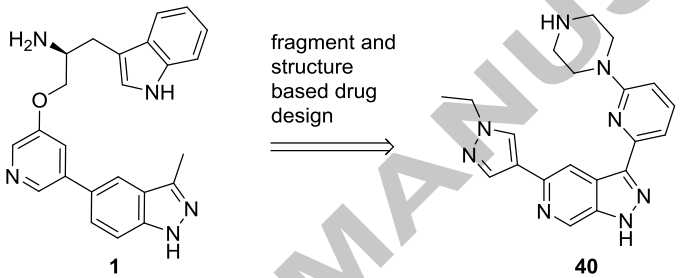

1

Ki (nM)
Pim-1: 13.8
Pim-2: 8.7
Pim-3: 16.7

40

Ki (nM)
Pim-1: 0.073
Pim-2: 0.473
Pim-3: 0.041